ACS Catalysis

Research Article

pubs.acs.org/acscatalysis

Mechanism and Kinetics of Ethanol Coupling to Butanol over Hydroxyapatite

Christopher R. Ho,[†,‡] Sankaranarayanapillai Shylesh,[†] and Alexis T. Bell*[,†,‡]

[†]Department of Chemical and Biomolecular Engineering, University of California, Berkeley, California 94720-1462, United States and
[‡]Chemical Sciences Division, Lawrence Berkeley National Laboratory, Berkeley, California 94720, United States

Supporting Information

ABSTRACT: The mechanism and kinetics for ethanol coupling to *n*-butanol over hydroxyapatite (HAP) were investigated at 573−613 K. *In situ* titration experiments show that the active sites for acetaldehyde and butanol formation are different. In combination with FTIR studies, it was found that ethanol dehydrogenation is catalyzed by Ca−O sites, whereas condensation of acetaldehyde is catalyzed by CaO/PO_4^{3-} pairs. Measurements of the reaction kinetics at various ethanol (3.5−9.4 kPa) and acetaldehyde (0.055−0.12 kPa) partial pressures reveal that direct condensation involving two ethanol molecules does not play a significant role in butanol formation; instead, *n*-butanol is formed via a Guerbet pathway. At a constant acetaldehyde pressure, enolate formation is rate-limiting, and ethanol inhibits acetaldehyde condensation rates by competitive adsorption. A model of the reaction kinetics consistent with all experimental observations is developed.

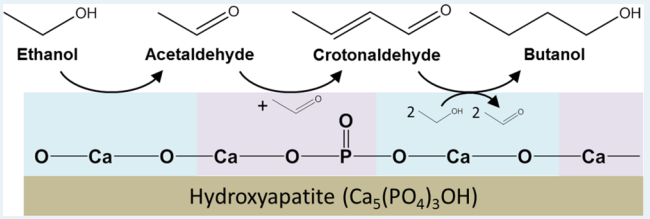

KEYWORDS: *hydroxyapatite, ethanol coupling, acetaldehyde, butanol, Guerbet reaction*

INTRODUCTION

Dramatic growth of U.S. ethanol production from biomass in recent years has motivated the search for efficient methods to upgrade ethanol to more valuable chemicals such as ethylene, 1,3-butadiene, and *n*-butanol.[1−3] Butanol is of particular interest because of its use for the production of products such as paints, solvents and polymers.[4] Moreover, because of its high energy density (29.2 MJ/L) and low miscibility with water, it is a superior biofuel to ethanol.[5] The traditional approach to producing butanol has been via the hydroformylation of propene followed by hydrogenation of the resulting butanal.[6,7]

More recently several investigators have shown that butanol can be produced via the coupling of ethanol over a variety of catalysts,[8,9] such as ruthenium complexes,[10] MgO,[11−13] Mg−Al mixed oxides,[14−17] Cu/CeO_2,[18] basic zeolites,[19] and hydroxyapatite.[20−25] Of these materials, hydroxyapatite is particularly noteworthy because it exhibits an unusually high activity and selectivity (>70%) to butanol.[21,23]

Hydroxyapatite (HAP; $Ca_5(PO_4)_3OH$) is a calcium phosphate that possesses both acid and base functionalities. Tsuchida et al. have shown using CO_2 TPD that increasing the Ca/P ratio of HAP leads to an increase in the density and strength of basic sites on the catalyst surface.[21] This trend also correlates well with an enhancement in the catalytic activity and selectivity toward butanol. Attempts to identify the catalytically active sites on HAP have relied largely on spectroscopic studies.[26−29] Diallo-Garcia et al. have observed the existence of basic OH^-, O^{2-}, and PO_4^{3-} groups through FTIR of adsorbed CO_2.[26,27] Further studies by these authors using acetylene as a probe have revealed an additional acid−base (POH−OH) pair.[27] Several authors have deduced from DRIFT spectra of ethanol adsorption at various temperatures the formation of weakly bound ethoxide species on POH groups, but the reactivity of these ethoxide species is currently unknown.[24,29]

Identification of acid sites has relied on FTIR spectroscopy of adsorbed pyridine. IR bands have been observed at around 1620, 1600, and 1440 cm^{-1}.[28,30−32] These bands are indicative of hydrogen- and coordinately bonded pyridine on Lewis acid sites. The absence of a band near 1540 cm^{-1} indicates the lack of Brønsted acid sites on HAP. FTIR spectra recorded at different temperatures show that pyridine desorbs completely by 473 K, implying that the Lewis acid sites to which pyridine is adsorbed are weak.[28,32] Hill et al. have obtained DRIFTS spectra on HAP with a variety of acid, base, and bifunctional probe molecules and found that both acid and base sites are weak compared to traditional metal oxide catalysts.[32] These authors have also shown, using steady-state isotopic transient kinetic analysis (SSITKA), that the active sites responsible for acetaldehyde formation are much fewer in number compared to the active sites responsible for butanol formation.[33]

While much is now known about the properties of hydroxyapatite, the composition and structure of the active sites responsible for ethanol coupling to butanol have not been clearly defined and neither has the mechanism for the reaction. Several groups have proposed that the reaction occurs via a Guerbet-type mechanism.[21,23,25] Ethanol is assumed to dehydrogenate to acetaldehyde, which then undergoes aldol condensation with another molecule of acetaldehyde to form

Received: November 25, 2015
Revised: December 22, 2015

DOI: 10.1021/acscatal.5b02672
ACS Catal. 2016, 6, 939−948

crotonaldehyde. Finally, the crotonaldehyde is doubly hydrogenated to form butanol. It is known from literature that hydroxyapatite is an active catalyst for alcohol dehydrogenation,[34,35] hydrogen transfer,[35] and aldol condensation,[36] which supports the Guerbet mechanism. However, other pathways have also been suggested, such as direct coupling of ethanol to either acetaldehyde or another ethanol molecule.[37] Gines et al. have shown that a Guerbet mechanism involving gas-phase acetaldehyde is not the only coupling pathway over $K-Cu_yMg_5CeO_x$ by observing unlabeled butanal in the presence of gaseous ^{13}C-labeled acetaldehyde.[38] More recently, Scalbert et al. have used thermodynamic arguments to show that in the Guerbet mechanism, gas phase hydrogen cannot be responsible for hydrogenation of the crotonaldehyde intermediate to butanol.[39,40] Ogo et al. have confirmed these results experimentally by demonstrating that crotonaldehyde does not undergo hydrogenation on HAP when gaseous H_2 is added to the feed.[22] This has led Scalbert et al. to support the direct condensation pathways, which are thermodynamically allowed.[39,40] However, the Guerbet mechanism is still a plausible pathway if crotonaldehyde is hydrogenated through a hydrogen transfer process involving ethanol.

The aim of this work is to elucidate the site requirements for ethanol coupling to butanol over HAP and the mechanism by which this process occurs. Our work suggests that the Guerbet pathway is the predominant route of ethanol coupling with the rate of reaction being limited by enolate formation. *In situ* titration and spectroscopic experiments point to the existence of two types of sites: basic Ca−O species that catalyze ethanol dehydrogenation and CaO/PO_4^{3-} pairs that catalyze acetaldehyde condensation. The reaction is shown to be autocatalytic with respect to acetaldehyde but is inhibited by ethanol adsorption over condensation sites. The data obtained in this study is used to develop a model for ethanol coupling to butanol over HAP.

EXPERIMENTAL METHODS

Catalyst Synthesis. Hydroxyapatite (HAP) was synthesized using a modification of the procedure reported by Tsuchida et al.[21] and Hanspal et al.[24] Aqueous solutions of 0.25 M $Ca(NO_3)_2{\cdot}4H_2O$ and 0.55 M $(NH_4)_2HPO_4$ were prepared and brought to a pH of 11 by addition of ammonium hydroxide. The calcium solution was added dropwise to the phosphorus solution at room temperature and stirred for 0.5 h before heating to 353 K for an additional 3 h. The resulting slurry was filtered, washed with DI water, and dried at 393 K overnight in air. The catalyst was calcined in 100 mL/min of air at 873 K for 2 h before use.

Calcium oxide was synthesized by a precipitation method using aqueous solutions of calcium chloride and sodium hydroxide to form the corresponding hydroxide before calcining at 773 K for 1 h.

Characterization Techniques. Powder X-ray diffraction (PXRD) patterns were taken with a Bruker D8 GADDS diffractometer equipped with a Cu−Kα source (40 kV, 40 mA). BET surface areas were calculated from nitrogen adsorption isotherms obtained using a Micromeritics Gemini VII 2390 surface area analyzer. The Ca/P ratio of HAP was determined by ICP-OES using an Optima 7000 DV instrument. Infrared spectra (FTIR) were acquired using a Thermo Scientific Nicolet 6700 spectrometer equipped with a liquid-nitrogen-cooled MCT detector. Samples were prepared by pressing 0.04 g of catalyst into a 20 mm-diameter pellet and placing it into a custom-built transmission cell with CaF_2 windows. All pellets for FTIR were pretreated in helium at 723 K overnight.

Measurements of Catalytic Activity. Measurements of reaction rates were carried out in a quartz-tube, packed-bed reactor (10 mm inner diameter). Quartz wool was placed below the catalyst bed to hold the catalyst in place. The reactor temperature was maintained using a tube furnace equipped with a Watlow temperature controller and a K-type thermocouple. Prior to reaction, the catalyst was treated in 50 mL min^{-1} of air (Praxair, zero grade) at 773 K for 1 h before cooling to the reaction temperature. This method was also used for catalyst regeneration.

In a typical experiment, ethanol (Sigma-Aldrich, 99.5%) and 10 vol % acetaldehyde (Sigma-Aldrich, 99.5%) in ethanol were introduced into a He (Praxair, 99.999%) stream flowing at 30 cm^3 min^{-1} using two syringe pumps (Cole Parmer, 74900 series). Propanol (Sigma-Aldrich, 99.8%), pyridine (Fisher Scientific, ACS grade), and propanoic acid (Sigma-Aldrich, 99.5%) were also fed in a similar manner. All experiments were carried out at a pressure of 1 atm. Product streams were analyzed by gas chromatography using an Agilent 6890A GC fitted with a HP-5 capillary column (30 m × 0.32 mm × 0.25 μm) and a flame ionization detector.

For studies of the reaction kinetics, the system was allowed to reach steady-state under a constant ethanol partial pressure of 5.7 kPa before introducing acetaldehyde into the feed stream. Since the addition of acetaldehyde causes slow catalytic deactivation, butanol formation rates were calculated by extrapolating rates to the time of acetaldehyde introduction. The conversion was calculated by summing all product yields. Selectivity was defined as the number of ethanol molecules consumed to form a product divided by the total amount of ethanol consumed. Yield was also defined on the basis of carbon number. Formation rates were calculated on the basis of moles of product, such that a 1:1 formation rate of acetaldehyde and butanol would ideally give a 1:2 yield because of the difference in carbon number. The carbon balance at an ethanol conversion of 17.1% was 95 ± 5% but was not precisely determined at very low ethanol conversions due to small fluctuations (~5%) in the feed rate of the syringe pumps. Acetaldehyde formation rates were determined by summing apparent acetaldehyde and butadiene formation rates since one molecule of acetaldehyde is consumed per molecule of butadiene produced. Reaction orders, model parameter values, and their associated errors were calculated by a least-squares regression analysis.

RESULTS AND DISCUSSION

The X-ray diffraction pattern of HAP shown in Figure 1a is characteristic of nanocrystalline apatite.[41,42] The IR spectrum of the catalyst presented in Figure 1b shows characteristic bands at 3572 (columnar OH^-) and 2200−1900 cm^{-1} (P−O overtone/combination modes) along with small bands at 1444 and 1414 cm^{-1} related to carbonate impurities.[26,43] The Ca/P ratio as measured by ICP-OES is 1.67, indicating a stoichiometric composition. The catalyst BET surface area is 81 m^2 g^{-1}.

Spacetime studies of ethanol conversion over HAP are shown in Figure 2. The yield of acetaldehyde reaches a plateau beyond 1/WHSV = 16 min, indicating that acetaldehyde is an intermediate for other products. The selectivity toward butanol reaches a maximum of 77% at an ethanol conversion of 8%. Above this conversion, the butanol selectivity decreases due to further coupling to form C6 alcohols. As shown in Table 1, several other products are observed in small quantities, most

DOI: 10.1021/acscatal.5b02672
ACS Catal. 2016, 6, 939−948

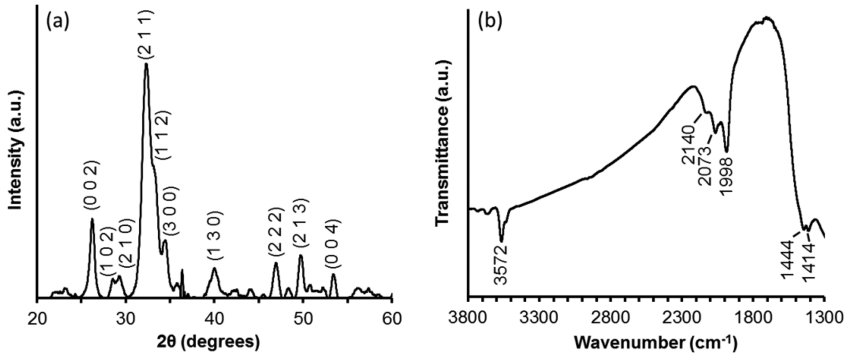

Figure 1. (a) XRD pattern and (b) IR spectrum of HAP. The main diffraction peaks of hydroxyapatite are labeled.

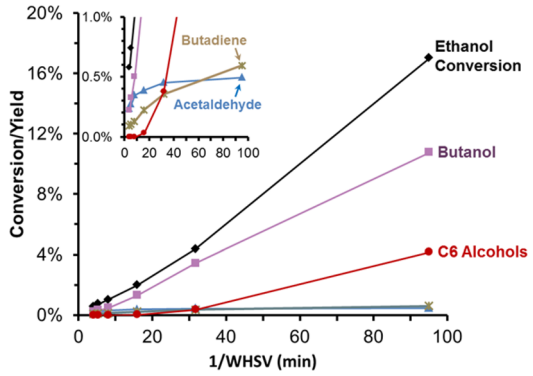

Figure 2. Effect of space velocity on ethanol conversion and product yields. Inset shows a vertically stretched region of the same plot. Solid lines are meant to guide the eye. T = 603 K; P_{EtOH} = 5.7 kPa; WHSV = w8 hly space velocity.

Table 1. Initial Ethanol Conversion and Product Selectivity over HAP[a]

catalyst	HAP
surface area (m^2/g)	81
conversion (%)	17.1
selectivity (%)	
ethylene	1.4
acetaldehyde	2.9
butadiene	3.5
butanol	63.2
crotonaldehyde	0.1
butanal	0.2
crotyl alcohol	0.7
C6+ alcohols	24.5

[a] T = 603 K; catalyst mass = 0.3 g; P_{EtOH} = 5.7 kPa; total gas flow rate at STP = 30 cm^3 min^{-1}.

notably crotonaldehyde, butanal, and crotyl alcohol, which are key intermediates in the Guerbet mechanism.

To gain more insight into the reaction pathway, several Guerbet intermediates (acetaldehyde, crotonaldehyde, butanal, crotyl alcohol) were fed into the reactor, and the conversions and product yields are shown in Table 2. In all cases, the carbon balance was poor, presumably due to the formation and deposition of heavy aldol oligomers on the catalyst surface. Quantitative conversion of acetaldehyde is achieved, with crotonaldehyde being the major observed product, demonstrating that aldol condensation proceeds rapidly under reaction conditions. When butanal is fed into the reactor, only trace amounts of crotyl alcohol and butanol are formed, indicating that intermolecular hydrogen transfer between two butanal molecules is slow. Similarly, a crotyl alcohol feed yields only trace amounts of crotonaldehyde and butanol. Instead, butadiene is formed in significant amounts, suggesting that crotyl alcohol preferentially undergoes a unimolecular dehydration reaction in the absence of a high concentration of a hydrogen donor such as ethanol.

Condensation and hydrogen transfer rates were compared by studying the reaction of acetaldehyde with 1-propanol over HAP using a method similar to that reported by Ogo et al.[22] 1-Propanol was chosen as the hydrogen donor because it is chemically similar to ethanol but does not convert to C2 products, which allows tracking of acetaldehyde consumption. The yield of ethanol (hydrogen transfer product) was 83%, while the yield of C5 alcohols (aldol condensation products) was 7%, showing that hydrogen transfer rates are much faster than aldol condensation rates, consistent with previous observations.[22] When 1-propanol is cofed with crotonaldehyde, butanal, or crotyl alcohol, butanol is the major product observed, showing that all three Guerbet intermediates can be readily reduced by a hydrogen donor. The fast hydrogen transfer rates also reduce the selectivity toward unwanted side reactions such as dehydration (in the case of crotyl alcohol) or further aldol condensation (in the case of crotonaldehyde and butanal). In the context of ethanol coupling to butanol, the results of these cofeed studies suggest that acetaldehyde formed by ethanol dehydrogenation easily undergoes aldol condensation to form crotonaldehyde. Crotonaldehyde is then rapidly hydrogenated to butanal, crotyl alcohol, and ultimately butanol, by hydrogen transfer with ethanol.

The apparent rates of acetaldehyde and butanol formation were measured as a function of ethanol partial pressure and are presented in Figure 3. The conversion ranged from 1% at high ethanol partial pressures to 5% at low ethanol partial pressures. The observed reaction order for acetaldehyde formation decreases from 1.0 to 0.3 ± 0.1 as ethanol partial pressure increases from 0.1 to 9.4 kPa. The rate of butanol formation is first order at low ethanol partial pressures (<1 kPa) and zero order at high ethanol partial pressures (9.4 kPa).

To assess the role of ethanol and acetaldehyde in the reaction more accurately, both reactants were cofed into the reactor to maintain constant ethanol and acetaldehyde partial pressures throughout the catalyst bed. Ethanol and acetaldehyde conversions were kept below 10% and 15% respectively to achieve differential conditions. Figure 4 shows butanol formation rates over HAP for a range of ethanol (3.5−9.4 kPa) and acetaldehyde

DOI: 10.1021/acscatal.5b02672
ACS Catal. 2016, 6, 939−948

Table 2. Conversion and Yield of Key Guerbet Intermediates over HAP[c]

		yield (%)								
reactant(s)	conversion (%)	ethanol	butadiene	crotonaldehyde	butanal	crotyl alcohol	butanol	C5 alcohols	C7 alcohols	other[b]
acetaldehyde	>99	0	0	17	0	0	0	-	-	2
crotonaldehyde	95	tr	0	-	0	0	0	-	-	58
butanal	90	tr	2	tr	-	tr	tr	-	-	37
crotyl alcohol	99	tr	32	tr	tr	-	tr	-	-	tr
acetaldehyde/1-propanol	>99[a]	0	0	0	0	0	83	7	0	-
crotonaldehyde/1-propanol	>99[a]	tr	4	-	tr	2	70	-	12	-
butanal/1-propanol	>99[a]	tr	8	tr	-	tr	61	-	23	-
crotyl alcohol/1-propanol	>99[a]	tr	8	tr	tr	-	68	-	15	-

[a]Conversions and yields based on the C2 or C4 reactant. [b]C6 aldehydes for acetaldehyde feed; C8 aldehydes for crotonaldehyde, butanal, and crotyl alcohol feeds. [c]T = 603 K; catalyst mass = 0.05 g; $P_{C2/C4\ molecules}$ = 0.1 kPa; $P_{1\text{-Propanol}}$ = 4.4 kPa; total gas flow rate at STP = 30 cm^3 min^{-1}. tr = trace (<1% yield).

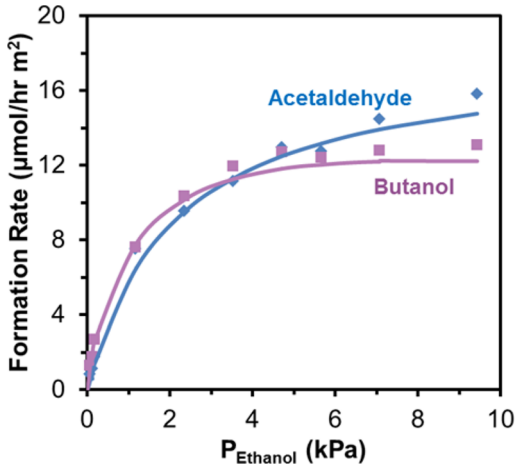

Figure 3. Rates of acetaldehyde and butanol formation as a function of ethanol partial pressure. The solid line for acetaldehyde represents the model fit from eq 1. The solid line for butanol represents the model fit from integrating eq 2 over the length of the reactor. T = 603 K; HAP mass = 0.05 g; total gas flow rate at STP = 30 cm^3 min^{-1}.

(0.055−0.12 kPa) partial pressures. For all reaction conditions tested, ethanol exhibits a negative order dependence (−0.4 to −0.7 ± 0.1), while acetaldehyde exhibits a positive order dependence (1.0 ± 0.2).

A direct coupling pathway involving two ethanol molecules would be expected to exhibit a zero to positive order in ethanol partial pressure based on a Langmuir−type mechanism and negative order dependence in acetaldehyde partial pressure due to competitive adsorption on the active sites. Instead, the opposite behavior is observed, indicating that the direct ethanol coupling pathway does not play a major role over HAP, although a pathway involving condensation between ethanol and acetaldehyde cannot be ruled out. In fact, linear extrapolation of butanol formation rates to P_{AA} = 0 kPa (Figure 4b) suggests that butanol does not form in the absence of gas-phase acetaldehyde. The rate enhancement by the addition of acetaldehyde demonstrates that acetaldehyde is an intermediate in the ethanol coupling reaction. When 87 μmol h^{-1} of acetaldehyde (0.12 kPa) is introduced into the ethanol feed stream, an additional 170 to 300 μmol h^{-1} of butanol is produced, depending on the ethanol partial pressure. This discrepancy in net acetaldehyde consumption and butanol formation rates strongly suggests that ethanol coupling is autocatalytic. The acetaldehyde consumed during the aldol condensation step must be regenerated during the reaction, implying that the hydrogenation step in the Guerbet pathway occurs via a hydrogen transfer mechanism between crotonaldehyde and ethanol. The first-order dependence on acetaldehyde suggests that enolate formation (rather than C−C coupling) is rate-limiting in the aldol condensation step.

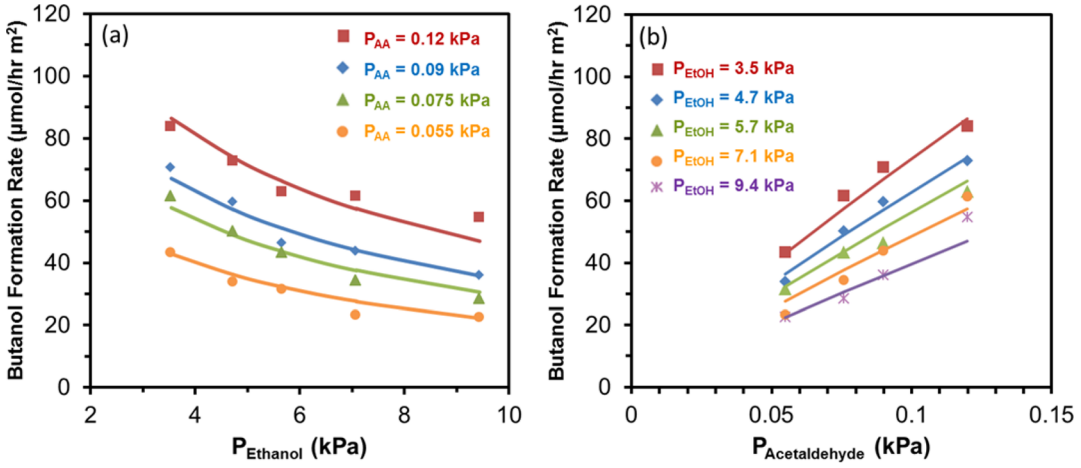

Figure 4. Butanol formation rates as a function of (a) ethanol partial pressure at constant acetaldehyde pressures and (b) acetaldehyde partial pressure at constant ethanol pressures. Solid lines represent the fitted kinetic model shown in eq 2. T = 603 K; HAP mass = 0.05 g; total gas flow rate at STP = 30 cm^3 min^{-1}. Abbreviations: EtOH = ethanol; AA = acetaldehyde.

DOI: 10.1021/acscatal.5b02672
ACS Catal. 2016, 6, 939−948

In situ titration experiments were performed over HAP to elucidate the site requirements for various products and intermediates. Pyridine was used to probe acidic sites, while carbon dioxide and propanoic acid were used to probe basic sites.

The change in acetaldehyde and butanol formation rates for two pyridine partial pressures is shown in Figure 5. Both rates

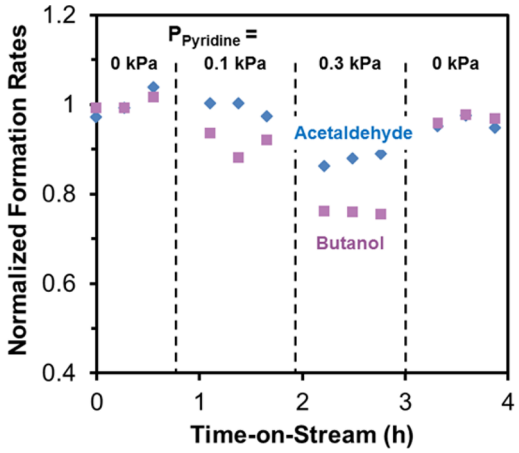

Figure 5. Transient formation rates of acetaldehyde and butanol over HAP during introduction and removal of pyridine. Rates are normalized to their initial steady-state values. T = 603 K; HAP mass = 0.05 g; P_{EtOH} = 5.7 kPa; total gas flow rate at STP = 30 cm^3 min^{-1}.

decrease slightly upon pyridine introduction and are rapidly restored by stopping the flow of titrant, suggesting that the acid sites on HAP are weak in nature, in agreement with reported IR observations.[28,30−32] Acetaldol was not detected in the product stream during the pyridine titration experiment, indicating that the dehydration step in acetaldehyde condensation to crotonaldehyde is fast, even in the presence of a titrant. Instead, the decrease in the rates of acetaldehyde and butanol formation upon pyridine addition suggest that weak acid sites such as Ca^{2+} or POH groups play a catalytic role by stabilizing reactive ethoxide and enolate intermediates formed on adjacent basic oxygen atoms.

The effects of *in situ* titration using CO_2 are shown in Figure 6. The acetaldehyde formation rate is unaffected by CO_2, whereas the butanol formation rate decreases by a factor of 5. Upon stopping the flow of CO_2, the butanol rate recovers back to 40% of its original value, indicating that a significant fraction of adsorbed CO_2 remains on the surface. When a stronger titrant such as propanoic acid is used, the rate of acetaldehyde formation decreases 6-fold, and the rate of butanol formation is completely suppressed (Figure S1). In addition, the butanol rate recovers much more slowly than the acetaldehyde rate. If HAP possesses a single active site that performs both unimolecular (dehydrogenation) and bimolecular (condensation) reaction, it would be expected that the identity of the titrant would not affect the relative selectivity of acetaldehyde and butanol as long as the same number of sites are titrated. However, this is not observed. The formation rate of butanol is strongly affected by the choice of titrant (Figure 5 − pyridine titration vs Figure 6 - CO_2 titration), while the formation rate of acetaldehyde does not change much. This suggests that the differences in transient responses for each of these titrants are due to the different site requirements for the formation of acetaldehyde and butanol.

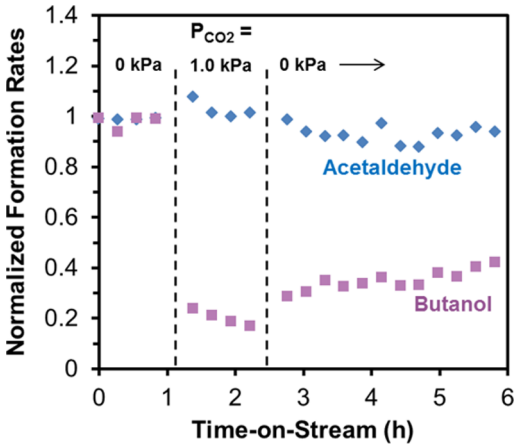

Figure 6. Transient formation rates of acetaldehyde and butanol over HAP during introduction and removal of CO_2. Rates are normalized to their initial steady-state values. T = 603 K; HAP mass = 0.1 g; P_{EtOH} = 5.7 kPa; total gas flow rate at STP = 60 cm^3 min^{-1}.

FTIR spectra of HAP acquired under a continuous flow of CO_2 (1 kPa) at 473 and 603 K are shown in Figure 7. The

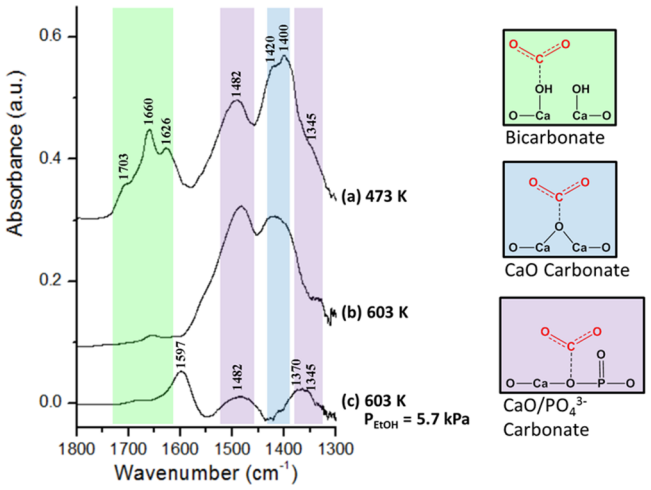

Figure 7. FTIR difference spectra of HAP upon introduction of continuous flow of P_{CO2} = 1 kPa at (a) 473 K, (b) 603 K, and (c) 603 K under continuous flow of P_{EtOH} = 5.7 kPa.

bands observed at 1703, 1660, and 1626 cm^{-1} at 473 K correspond to surface bicarbonate species formed by reaction of CO_2 with Ca−OH groups.[27,32] The bands at 1482 and 1345 cm^{-1} can be assigned to surface carbonates bound to phosphate groups, whereas the bands at 1420 and 1400 cm^{-1} are related to carbonate species on Ca−O sites derived from condensation of two adjacent surface Ca−OH groups.[27,43] At 603 K, the bicarbonate species disappear, but the surface carbonates remain, indicating that most Ca−OH surface groups have been converted to Ca−O.[43]

Figure 7 also shows difference spectra for HAP taken in the presence of a continuous ethanol feed after introduction of CO_2. The reaction conditions (T = 603 K, P_{EtOH} = 5.7 kPa, P_{CO2} = 1.0 kPa) were identical to those used in the *in situ* CO_2 titration experiment. The bands at 1420 and 1400 cm^{-1} disappear, demonstrating that ethanol effectively displaces CO_2 from Ca−O sites. This suggests that ethanol dehydrogenation occurs over these sites because CO_2 does not inhibit the

DOI: 10.1021/acscatal.5b02672
ACS Catal. 2016, 6, 939−948

formation of acetaldehyde. On the other hand, the bands at 1482 and 1345 cm^{-1} remain, indicating that CO_2 is still adsorbed on phosphate groups. A new band at 1370 cm^{-1} is observed, which can also be assigned to carbonates species associated with phosphate groups.[27] This band is likely also present in the two spectra of CO_2-adsorbed HAP shown in Figure 7 but is buried under the broad band at 1400 cm^{-1}. Another new band at 1597 cm^{-1} is also seen, which can be assigned to bidentate carbonate species that can be formed from acid−base pairs.[32] All of these bands point to the presence of a Ca−O−P site that can form carbonates adsorbed on phosphate groups. The observed decrease in butanol formation rate upon introduction of CO_2 can thus be attributed to the blockage of these Ca−O−P sites by formation of surface carbonate species.

To develop a mechanism for ethanol coupling to butanol over HAP, it is first necessary to envision the structure of the catalyst surface. Prior studies have shown that the morphology and surface functionality of HAP are highly dependent on synthesis conditions.[44] HAP synthesized by coprecipitation in basic media preferentially exposes basic surface facets due to favorable solvation effects.[45] Ospina et al. have synthesized stoichiometric HAP at pH = 11 and observed the predominance of the basic hydroxyl-terminated (010) plane using high-resolution transmission electron microscopy.[41] Under less basic synthesis conditions (pH < 10), HAP exposes fewer basic sites which leads to a reduction in catalytic activity and selectivity toward butanol.[21] This suggests that basic crystal planes, such as the hydroxyl-terminated (010) plane, are responsible for the chemistry. Figure 8 illustrates this surface possesses Ca−OH

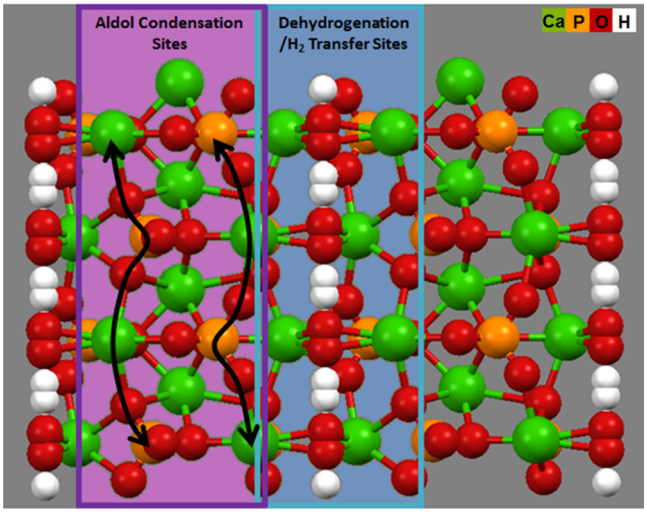

Figure 8. Top-down view of the hydroxyl-terminated (010) plane showing four unit cells. The image was generated from diffraction data reported by Hughes et al.[46] using the molecular graphics program MECURY.[47] Green is calcium, orange is phosphorus, red is oxygen, and white is hydrogen. The blue-shaded region corresponds to dehydrogenation/hydrogen transfer sites, while the purple-shaded region corresponds to aldol condensation sites. Black arrows indicate the surface atoms involved in aldol condensation.

sites needed for ethanol dehydrogenation as well as CaO/PO_4^{3-} pairs needed for aldol condensation.

The first step of ethanol coupling to butanol involves the dehydrogenation of ethanol to acetaldehyde via an E_{1cB} mechanism, as proposed by Kibby et al. and Tsuchida et al.[21,35]

Scheme 1. Reaction Mechanism for Ethanol Dehydrogenation to Acetaldehyde over HAP

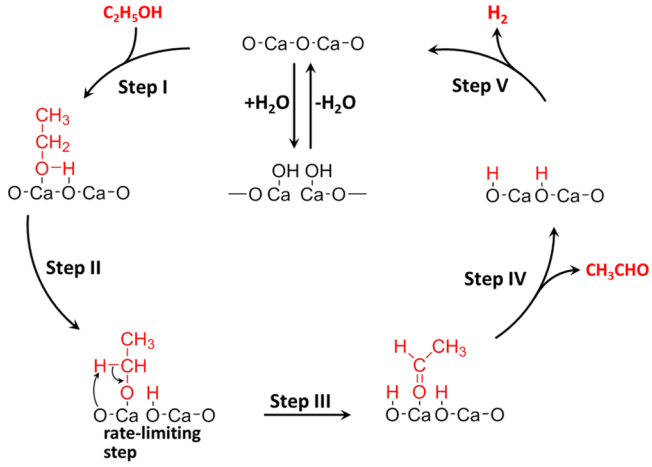

As shown in Scheme 1, this mechanism starts with dissociative adsorption of ethanol on Ca−O sites to form surface ethoxide and hydroxyl species (Step I, Scheme 1). This is followed by abstraction of an α-hydrogen atom by surface oxygen in what is thought to be the rate-limiting step for dehydrogenation (Step II, Scheme 1) and electron transfer to the C_α-O bond to form the adsorbed acetaldehyde which then desorbs (Steps III−IV, Scheme 1). The remaining hydrogen adatoms combine to form H_2 gas (Step V, Scheme 1).

Once acetaldehyde is formed, it can migrate to the neighboring CaO/PO_4^{3-} sites responsible for aldol condensation. This mechanism is initiated by adsorption of acetaldehyde onto the surface (Step I, Scheme 2). The next step is rate-limiting in the aldol condensation process and involves the abstraction of an α-hydrogen by a basic oxygen to form an enolate species (Step II, Scheme 2). The enolate is stabilized by the nearby phosphate group which is weakly acidic. This acid−base cooperation accelerates aldol condensation rates and has been observed over other catalytic systems such as mixed Mg−Al oxides or grafted amines.[16,48] The enolate adds to the carbonyl group of another acetaldehyde molecule to form acetaldol (Step III, Scheme 2) which dehydrates to form crotonaldehyde (Step IV, Scheme 2). Desorption of crotonaldehyde and water (Steps V−VI, Scheme 2) completes the catalytic cycle. Ethanol does not participate directly in the reaction but can adsorb onto the active site and thereby inhibit the aldol condensation process.

Crotonaldehyde is hydrogenated to butanol by hydrogen transfer from ethanol. The possible mechanisms for hydrogen transfer can be divided into three categories based on the form of the exchanged hydrogen (H_2 gas, surface hydrogen adatoms, or direct hydrogen transfer). Ogo et al. demonstrated that a crotonaldehyde/H_2 feed does not produce any hydrogen transfer products over HAP, ruling out H_2 gas as the hydrogenation source.[22] Furthermore, the addition of acetaldehyde to an ethanol feed increases crotonaldehyde hydrogen transfer rates over HAP (Figure 4), showing that the reaction does not proceed by indirect transfer of surface hydrogen in which deposition of surface hydrogen from ethanol is rate-limiting. Instead, hydrogenation of crotonaldehyde is envisioned to occur by a direct hydrogen transfer mechanism. This can proceed via a Meerwein-Ponndorf-Verley (MPV) reduction with ethanol to yield crotyl alcohol, shown in Scheme 3. Crotyl

DOI: 10.1021/acscatal.5b02672
ACS Catal. 2016, 6, 939−948

Scheme 2. Reaction Mechanism for Aldol Condensation of Acetaldehyde to Crotonaldehyde over HAP

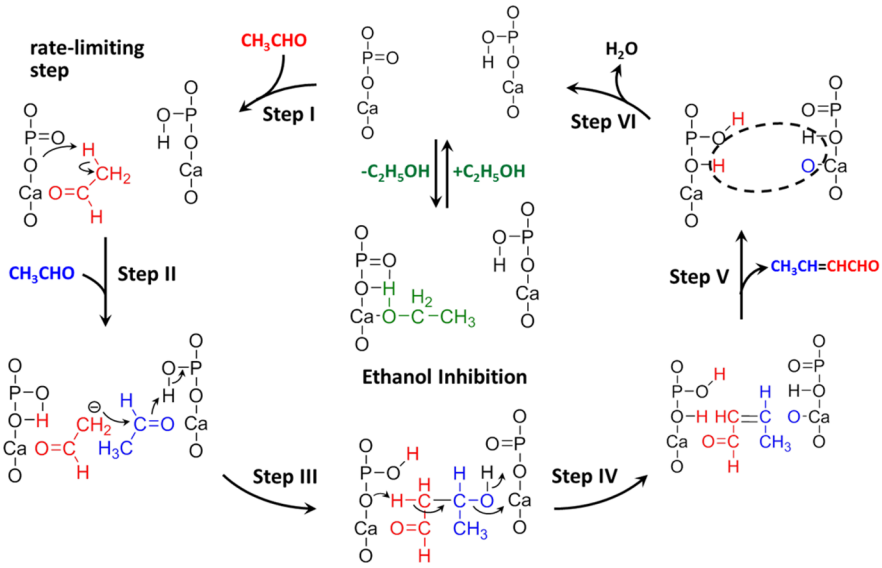

Scheme 3. Hydrogen Transfer Pathway between Crotonaldehyde and Ethanol

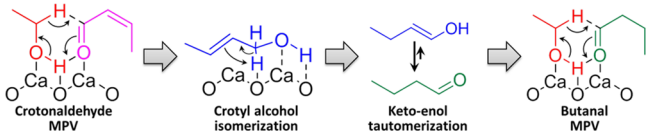

alcohol subsequently isomerizes to 1-buten-1-ol by abstraction and relocation of the α-hydrogen by basic oxygen to form an enol which tautomerizes into butanal. A second MPV reduction converts butanal to butanol. This hydrogen transfer mechanism is hypothesized to occur on Ca−O sites as calcium oxide is known to catalyze C═C isomerization and MPV reduction.[49,50] When 0.12 kPa of crotonaldehyde is fed over calcium oxide in the presence of excess propanol at 330 °C, butanol is formed selectively (97% yield), providing further evidence that Ca−O is the active site for hydrogen transfer over HAP (Table S2).

The entire mechanism can be condensed into the reaction pathway shown in Scheme 4. This scheme depicts ethanol

Scheme 4. Proposed Reaction Pathway for the Guerbet Coupling of Ethanol to Butanol over the HAP Catalyst

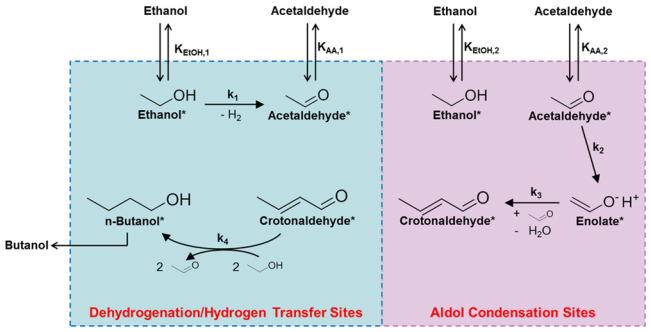

dehydrogenation to acetaldehyde on Ca−O sites, acetaldehyde condensation to crotonaldehyde on CaO/PO_4^{3-} pairs, and hydrogen transfer between ethanol and crotonaldehyde to form butanol. The selectivity between acetaldehyde and butanol is dictated by the relative rates of dehydrogenation and aldol condensation. Acetaldehyde formation exhibits a positive but less than first-order dependence on ethanol partial pressure which is consistent with the E_{1cB} mechanism.

Using a Langmuir model, a rate expression for acetaldehyde formation can be derived based on the proposed mechanism and is given in eq 1.

$$r_{AA} = \frac{k_1 K_{EtOH,1} P_{EtOH}}{1 + K_{EtOH,1} P_{EtOH}} \quad (1)$$

The parameter k_1 is an effective rate constant associated with the abstraction of the α-hydrogen from ethanol, while $K_{EtOH,1}$ is the equilibrium constant for ethanol adsorption onto Ca−O sites. The formation of butanol does not affect the rate expression for acetaldehyde since the consumption of acetaldehyde in the aldol condensation step is balanced by the generation of acetaldehyde in the subsequent hydrogen transfer reactions. Values of k_1 = 18 μmol/h·m^2 and $K_{EtOH,1}$ = 0.48 kPa^{-1} result in a very good description of the rate of acetaldehyde formation, as shown in Figure 3.

Similarly, a rate expression for butanol formation can be derived based on the mechanism presented in Scheme 2. The observed negative order dependence in ethanol and first-order dependence in acetaldehyde for butanol formation indicate that empty sites and adsorbed ethanol molecules are the most predominant surface species on the aldol condensation sites. Application of the pseudo-steady-state approximation to all surface intermediates results in the simplified rate expression given by eq 2.

$$r_{BuOH} = \frac{k_2 K_{AA,2} P_{AA}}{1 + K_{EtOH,2} P_{EtOH}} \quad (2)$$

$P_{AA/EtOH}$ is the partial pressure of acetaldehyde/ethanol, k_2 is the rate constant for enolate formation, and $K_{AA,2/EtOH,2}$ are the equilibrium constants for acetaldehyde and ethanol adsorption presented in Scheme 4. Values of $k_2K_{AA,2}$ = 1500 μmol/h·m^2·kPa and $K_{EtOH,2}$ = 0.30 kPa^{-1} accurately capture the rate of butanol formation, as shown in Figure 4.

The temperature dependence of all rate and adsorption equilibrium constants were obtained by fitting eqs 1 and 2 to rate data obtained at various temperatures (573−613 K).

DOI: 10.1021/acscatal.5b02672
ACS Catal. 2016, 6, 939−948

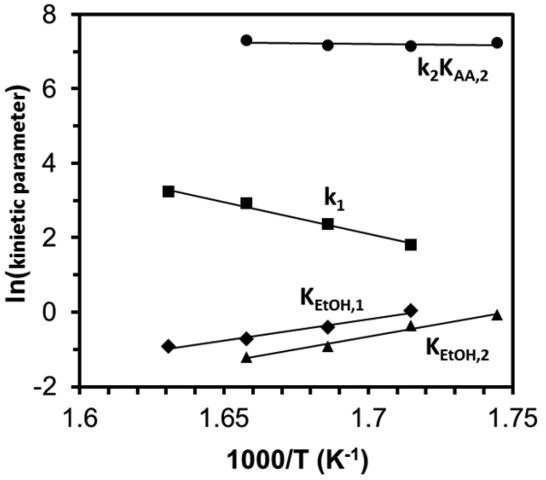

Figure 9. Arrhenius plots for ethanol dehydrogenation and aldol condensation reactions over HAP.

These results are depicted in Figure 9. Apparent activation energies and heats of adsorption calculated in this manner are given in Table 3. The enthalpies of adsorption for ethanol over dehydrogenation ($\Delta H_{EtOH,1}$) and aldol condensation ($\Delta H_{EtOH,2}$) sites are both approximately −25 kcal/mol, in good agreement with adsorption microcalorimetric measurements reported by Hanspal et al. (−22 to −26 kcal/mol).[24] The lumped parameter $k_2K_{AA,2}$ has an apparent activation energy of 1.8 ± 2.5 kcal/mol, indicating that the heat of adsorption of acetaldehyde is roughly equal to the activation barrier for enolate formation on aldol condensation sites. The activation energy for ethanol dehydrogenation (E_1) is 34 ± 2 kcal/mol, which is 12 kcal/mol higher than the reported activation energy for 2-butanol dehydrogenation over HAP.[35] This difference is a direct consequence of the relative stability between acetaldehyde and 2-butanone. Ketones formed from secondary alcohols have two methyl groups that stabilize the carbonyl bond compared to the one methyl group for the more reactive aldehydes.

Parity plots comparing measured formation rates and those obtained from eqs 1 and 2 are shown for acetaldehyde and butanol in Figure 10. The data points cluster along the diagonal, which indicates a good description of the data by the model.

The model also explains the kinetics observed when only ethanol is fed into the reactor. At low ethanol partial pressures (<4 kPa), acetaldehyde can freely adsorb on aldol condensation sites. Thus, the positive order dependence for butanol formation is a direct consequence of the positive order dependence for ethanol dehydrogenation. As ethanol partial pressure increases, ethanol begins to compete with acetaldehyde for adsorption on the condensation sites. As a result, aldol condensation rates decrease and oppose the increasing dehydrogenation rates, leading to the observed zero-order dependence for butanol formation at high ethanol partial pressures.

The apparent rate of butanol formation from a pure ethanol feed can be predicted by integrating the rate expression given in eq 2 over the length of the catalyst bed, as shown in eq 3.

$$r_{BuOH,app} = \frac{1}{L'}\int_0^{L'} r_{BuOH}\,dL = \frac{1}{L'}\frac{k_2K_{AA,2}}{1 + K_{EtOH,2}P_{EtOH}}\int_0^{L'} P_{AA}\,dL \tag{3}$$

$r_{BuOH,app}$ is the apparent butanol formation rate, r_{BuOH} is the local rate of butanol formation at a distance L from the top of the catalyst bed, and L' is the total length of the bed. The partial pressure of ethanol was taken to be constant because the experiments were performed under differential conditions (<5% conversion). The spatial dependence of acetaldehyde partial pressure was determined experimentally through spacetime studies (Figure 2) to account for minor acetaldehyde-consuming

Table 3. Apparent Activation Energies and Pre-Exponential Factors for Ethanol Dehydrogenation and Aldol Condensation over HAP Based on a Least Squares Regression Analysis with the Data Presented in Figure 9

parameter	k_1 (μmol/h·m^2)	$K_{EtOH,1}$ (kPa^{-1})	$k_2K_{AA,2}$ (μmol/h·m^2·kPa)	$K_{EtOH,2}$ (kPa^{-1})
apparent E_a or ΔH_{ads} (kcal/mol)	34 ± 2	−23 ± 2	1.8 ± 2.5	−27 ± 3
ln(A)	31 ± 2	−19 ± 2	8.7 ± 2.1	−24 ± 3

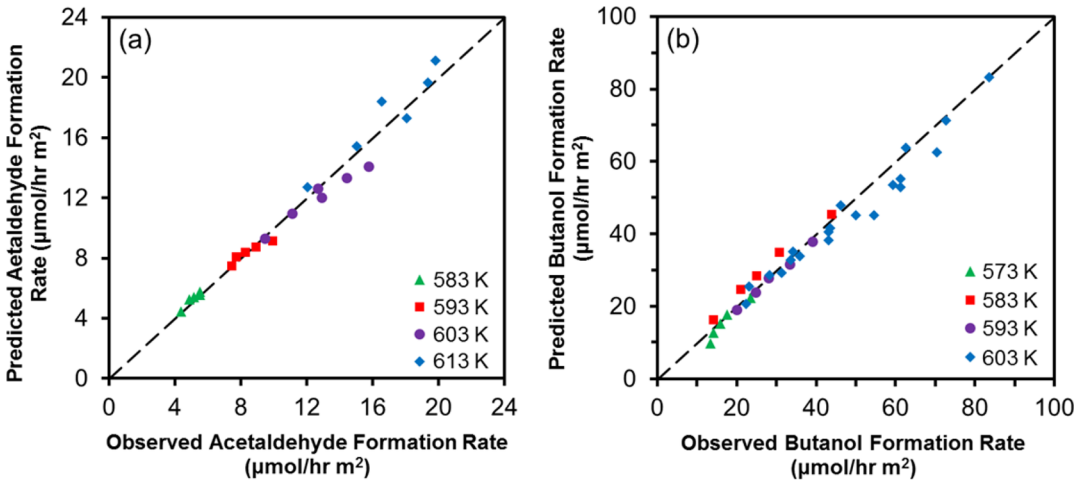

Figure 10. Parity plots for rates of (a) acetaldehyde and (b) butanol formation derived from kinetic data and eqs 1 and 2. P_{EtOH} = 2.4−9.4 kPa; P_{AA} = 0.055−0.12 kPa; T = 573−613 K; HAP mass = 0.05 g; total gas flow rate = 30 cm^3 min^{-1}.

DOI: 10.1021/acscatal.5b02672
ACS Catal. 2016, 6, 939−948

side reactions such as the formation of butadiene. As shown in Figure 3, the model developed from ethanol/acetaldehyde cofeed kinetics accurately predicts butanol formation rates.

CONCLUSIONS

Butanol formation rates on HAP were determined over a range of ethanol (3.5−9.4 kPa) and acetaldehyde (0.055−0.12 kPa) partial pressures. A strong increase in the rate butanol formation was observed upon addition of acetaldehyde to the feed, demonstrating that the reaction is autocatalytic. For all reaction conditions tested, ethanol exhibits a negative order dependence, while acetaldehyde exhibits a positive, first-order dependence, implying that butanol is formed via a Guerbet-type mechanism involving sequential dehydrogenation, aldol condensation, and hydrogen transfer reactions.

Poisoning experiments with CO_2 and propionic acid reveal that acetaldehyde and butanol formation rates decrease to different extents, demonstrating that the sites for the two reactions are not equivalent. Combined with in situ FTIR results, it was found that dehydrogenation is catalyzed by Ca−O groups, while aldol condensation requires calcium oxide/phosphate pairs. A detailed model of ethanol coupling reaction was developed that accurately describes all experimental observations.

ASSOCIATED CONTENT

Supporting Information

The Supporting Information is available free of charge on the ACS Publications website at DOI: 10.1021/acscatal.5b02672.

Figure S1, propionic acid titration data; Figure S2, PXRD spectra of spent HAP; Table S1, initial ethanol conversion and product selectivity over calcium oxide; Table S2, conversion of Guerbet intermediates over calcium oxide (PDF)

AUTHOR INFORMATION

Corresponding Author

*E-mail: bell@cchem.berkeley.edu.

Notes

The authors declare no competing financial interest.

ACKNOWLEDGMENTS

This work was funded by Director, Office of Science, Office of Basic Energy Sciences of the U.S. Department of Energy under Contract No. DE-AC02-05CH11231. The authors would like to thank Joseph Gomes for helpful discussions.

REFERENCES

(1) Sun, J.; Wang, Y. *ACS Catal.* **2014**, *4*, 1078−1090.
(2) DeWilde, J. F.; Chiang, H.; Hickman, D. A.; Ho, C. R.; Bhan, A. *ACS Catal.* **2013**, *3*, 798−807.
(3) Jones, M. D. *Chem. Cent. J.* **2014**, *8*, 1−5.
(4) Ash, M.; Ash, I. *Handbook of green chemicals*, 2nd ed.; Synapse Information Resources: Endicott, 2004; pp 645−646.
(5) Cheng, J. *Biomass to Renewable Energy Processes*; CRC Press: Boca Raton, 2010; pp 272−273.
(6) Van Leeuwen, P. W. N. M.; Claver, C. *Rhodium Catalyzed Hydroformylation*; Kuwer Academic Publishers: Dordrecht, 2000; pp 6−8.
(7) Weissermel, K.; Arpe, H.-J. *Industrial Organic Chemistry*, 4th ed.; Wiley-VCH: New York, 2003; pp 127−138.
(8) Kozlowski, J. T.; Davis, R. J. *ACS Catal.* **2013**, *3*, 1588−1600.
(9) Gabriëls, D.; Hernández, W. Y.; Sels, B.; Van Der Voort, P.; Verberckmoes, A. *Catal. Sci. Technol.* **2015**, *5*, 3876−3902.
(10) Dowson, G. R. M.; Haddow, M. F.; Lee, J.; Wingad, R. L.; Wass, D. F. *Angew. Chem., Int. Ed.* **2013**, *52*, 9005−9008.
(11) Ueda, W.; Ohshida, T.; Kuwabara, T.; Morikawa, Y. *Catal. Lett.* **1992**, *12*, 97−104.
(12) Ndou, A. S.; Plint, N.; Coville, N. J. *Appl. Catal., A* **2003**, *251*, 337−345.
(13) Birky, T. W.; Kozlowski, J. T.; Davis, R. J. *J. Catal.* **2013**, *298*, 130−137.
(14) León, M.; Díaz, E.; Ordóñez, S. *Catal. Today* **2011**, *164*, 436−442.
(15) Carvalho, D. L.; de Avillez, R. R.; Rodrigues, M. T.; Borges, L. E. P.; Appel, L. G. *Appl. Catal., A* **2012**, *415*−*416*, 96−100.
(16) Di Cosimo, J. I.; Díez, V. K.; Xu, M.; Iglesia, E.; Apesteguía, C. R. *J. Catal.* **1998**, *178*, 499−510.
(17) Di Cosimo, J. I.; Apesteguía, C. R.; Ginés, M. J. L.; Iglesia, E. *J. Catal.* **2000**, *190*, 261−275.
(18) Earley, J. H.; Bourne, R.; Poliakoff, M.; Watson, M. *Green Chem.* **2015**, *17*, 3018−3025.
(19) Yang, C.; Meng, Z. *J. Catal.* **1993**, *142*, 37−44.
(20) Tsuchida, T.; Sakuma, S.; Takeguchi, T.; Ueda, W. *Ind. Eng. Chem. Res.* **2006**, *45*, 8634−8642.
(21) Tsuchida, T.; Kubo, J.; Yoshioka, T.; Sakuma, S.; Takeguchi, T.; Ueda, W. *J. Catal.* **2008**, *259*, 183−189.
(22) Ogo, S.; Onda, A.; Yanagisawa, K. *Appl. Catal., A* **2011**, *402*, 188−195.
(23) Ogo, S.; Onda, A.; Iwasa, Y.; Hara, K.; Fukuoka, A.; Yanagisawa, K. *J. Catal.* **2012**, *296*, 24−30.
(24) Hanspal, S.; Young, Z. D.; Shou, H.; Davis, R. J. *ACS Catal.* **2015**, *5*, 1737−1746.
(25) Silvester, L.; Lamonier, J.-F.; Faye, J.; Capron, M.; Vannier, R.-N.; Lamonier, C.; Dubois, J.; Couturier, J.; Calais, C.; Dumeignil, F. Y. *Catal. Sci. Technol.* **2015**, *5*, 2994−3006.
(26) Diallo-Garcia, S.; Osman, M. B.; Krafft, J. M.; Boujday, S.; Guylène, C. *Catal. Today* **2014**, *226*, 81−88.
(27) Diallo-Garcia, S.; Osman, M. B.; Krafft, J. M.; Casale, S.; Thomas, C.; Kubo, J.; Costentin, G. *J. Phys. Chem. C* **2014**, *118*, 12744−12757.
(28) Stošić, D.; Bennici, S.; Sirotin, S.; Calais, C.; Couturier, J.-L.; Dubois, J.-L.; Travert, A.; Auroux, A. *Appl. Catal., A* **2012**, *447*−*448*, 124−134.
(29) Ramesh, K.; Goh, E.; Ling, Y.; Gwie, C. G.; White, T. J.; Borgna, A. *J. Phys. Chem. C* **2012**, *116*, 18736−18745.
(30) Parry, E. *J. Catal.* **1963**, *2*, 371−379.
(31) Tanaka, H.; Watanabe, T.; Chikazawa, M. *J. Chem. Soc., Faraday Trans.* **1997**, *93*, 4377−4381.
(32) Hill, I. M.; Hanspal, S.; Young, Z. D.; Davis, R. J. *J. Phys. Chem. C* **2015**, *119*, 9186−9197.
(33) Hanspal, S.; Young, Z. D.; Shou, H.; Davis, R. J. *ACS Catal.* **2015**, *5*, 1737−1746.
(34) Kibby, C. L.; Hall, W. *J. Catal.* **1973**, *29*, 144−159.
(35) Kibby, C. L.; Hall, W. *J. Catal.* **1973**, *31*, 65−73.
(36) Rodrigues, E. G.; Keller, T. C.; Mitchell, S.; Pérez-Ramírez, J. *Green Chem.* **2014**, *16*, 4870−4874.
(37) Chieregato, A.; Ochoa, J. V.; Bandinelli, C.; Fornasari, G.; Cavani, F.; Mella, M. *ChemSusChem* **2015**, *8*, 377−388.
(38) Gines, M.; Iglesia, E. *J. Catal.* **1998**, *176*, 155−172.
(39) Scalbert, J.; Thibault-Starzyk, F.; Jacquot, R.; Morvan, D.; Meunier, F. *J. Catal.* **2014**, *311*, 28−32.
(40) Meunier, F. C.; Scalbert, J.; Thibault-Starzyk, F. *C. R. Chim.* **2015**, *18*, 345−350.
(41) Ospina, C. a; Terra, J.; Ramirez, A. J.; Farina, M.; Ellis, D. E.; Rossi, A. M. *Colloids Surf., B* **2012**, *89*, 15−22.
(42) Mobasherpour, I.; Heshajin, M. S.; Kazemzadeh, a.; Zakeri, M. *J. Alloys Compd.* **2007**, *430*, 330−333.
(43) Cheng, Z.; Yasukawa, A.; Kandori, K.; Ishikawa, T. *Langmuir* **1998**, *14*, 6681−6686.
(44) Liu, J.; Ye, X.; Wang, H.; Zhu, M.; Wang, B.; Yan, H. *Ceram. Int.* **2003**, *29*, 629−633.
(45) Slepko, A.; Demkov, A. A. *J. Chem. Phys.* **2013**, *139*, 044714.

DOI: 10.1021/acscatal.5b02672
ACS Catal. 2016, 6, 939−948

(46) Hughes, J. M.; Cameron, M.; Crowley, K. D. *Am. Mineral.* **1989**, *74*, 870−876.
(47) Macrae, C. F.; Edgington, P. R.; McCabe, P.; Pidcock, E.; Shields, G. P.; Taylor, R.; Towler, M.; Van De Streek, J. *J. Appl. Crystallogr.* **2006**, *39*, 453−457.
(48) Shylesh, S.; Hanna, D.; Gomes, J.; Krishna, S.; Canlas, C. G.; Head-Gordon, M.; Bell, A. T. *ChemCatChem* **2014**, *6*, 1283−1290.
(49) Aramendía, M. A.; Borau, V.; Jiménez, C.; Marinas, J. M.; Ruiz, J. R.; Urbano, F. J. *J. Colloid Interface Sci.* **2001**, *238*, 385−389.
(50) Schächter, Y.; Pines, H. *J. Catal.* **1968**, *11*, 147−158.

DOI: 10.1021/acscatal.5b02672
ACS Catal. 2016, 6, 939−948